The Astrophysical Journal, 625:278–290, 2005 May 20

EFFECTS OF A BLACK HOLE'S GRAVITATIONAL FIELD ON THE LUMINOSITY OF A STAR DURING A CLOSE ENCOUNTER

Andreja Gomboc[1,2] and Andrej Čadež[1]
Received 2004 April 22; accepted 2005 January 29

ABSTRACT

To complement hydrodynamic studies of the tidal disruption of the star by a massive black hole, we present the study of stellar luminosity and its variations produced by the strong gravitational field of the black hole during a close encounter. By simulating the relativistically moving star and its emitted light and taking into account general relativistic effects on particle and light trajectories, our results show that the black hole's gravity alone induces apparent stellar luminosity variations on typical timescales of a few r_g/c [=(5 s)$m_{\rm bh}/(10^6\ M_\odot)$] to a few 100 r_g/c [$\sim$(10 minutes)$m_{\rm bh}/(10^6\ M_\odot)$], where $r_g = Gm_{\rm bh}/c^2$. We discern different cases with respect to the strength of tidal interaction and focus on two: (1) a star encountering a giant black hole traces spacetime almost as a point particle, so the apparent luminosity variations are dominated by clearly recognizable general relativistic effects, and (2) in a close encounter of a star with a black hole of similar size, the stellar debris is spread around the black hole by processes in which hydrodynamics plays an important role. We discuss limitations and results of our approach.

Subject headings: black hole physics — hydrodynamics

1. INTRODUCTION

Motivation for our work comes from the presence of massive black holes in galactic nuclei and from the possibility that such black holes accrete material from their surroundings. It was estimated (Gurzadyan & Ozernoy 1981; Rees 1990; Magorrian & Tremaine 1999; Syer & Ulmer 1999) that central black holes may capture stars from inner galactic regions at the rate from 10^{-3} to 10^{-7} stars per galaxy per year. Such events would be particularly interesting in the Galactic center, where the observed X-ray flare (Baganoff et al. 2001) and measured motion of stars, down to only 17 lt-hr from the center (Schödel et al. 2002), provide strong evidence that the central concentration of about $3 \times 10^6\ M_\odot$ is indeed a black hole. In recent years UV and X-ray flares have been observed in the nuclei of NGC 4552, NGC 5905, RX J1242.6−1119, RX J1624.9+7554, and others, for which it was concluded that tidal disruption of a star by a massive black hole provides the best explanation (Renzini et al. 1995; Komossa & Bade 1999; Grupe et al. 1999; Gezari et al. 2003).

The interaction of a star with a black hole has been studied previously by other authors (Rees 1988; Carter & Luminet 1985; Luminet & Marck 1985) with a number of detailed hydrodynamic simulations (Laguna et al. 1993; Khokhlov et al. 1993a, 1993b; Kochanek 1994; Fulbright et al. 1995; Marck et al. 1996; Diener et al. 1997; Loeb & Ulmer 1997; Ayal et al. 2000; Ivanov & Novikov 2001; Ivanov et al. 2003) with emphasis on stellar structure during the encounter with the black hole and long-term evolution of stellar debris. Nevertheless, none of these studied the luminosity variations occurring to the star in the vicinity of the black hole. In order to be complete, such a study should include stellar hydrodynamics in full general relativity, modeling of radiation processes in the disrupted star, and relativistic effects on the emitted light. Because of the complexity of the subject, we do not attempt to study all these effects in full here, but we wish to complement hydrodynamic studies by previously mentioned authors. Therefore, we limit our attention in this paper to effects on a star's luminosity induced solely by the gravity of the black hole, as we expect that relativistic effects alone might produce interesting luminosity phenomena. We simulate the disruption and the appearance of the star during a close encounter as it would be seen by a distant observer and make a comparison of some results in our model with those obtained by hydrodynamic simulations.

The model of the star used in our simulations depends on the expected strength of the tidal interactions between the star and black hole. Tidal disruption of the star with mass M_* and radius R_* occurs only if the star approaches the black hole to within its Roche radius:

$$r_{\rm R} = \left(\frac{m_{\rm bh}}{M_*}\right)^{1/3} R_*, \tag{1}$$

which, expressed in units of the black hole's gravitational radius $r_g = Gm_{\rm bh}/c^2$, reads

$$\mathcal{R}_{\rm R} = \frac{r_{\rm R}}{2r_g} = 25\left(\frac{\rho_\odot}{\rho_*}\right)^{1/3}\left(\frac{10^6\ M_\odot}{m_{\rm bh}}\right)^{2/3}, \tag{2}$$

where $\rho_\odot$ and ρ_* are the average densities of the Sun and the star, respectively. It is convenient to introduce the dimensionless Roche radius penetration factor $\beta = r_{\rm R}/r_p$, where r_p is the periastron distance of the star with respect to the black hole. The Roche penetration factor of a black hole grazing orbit is obviously $\beta_{\rm gr} = r_{\rm R}/(2r_g + R_*) = \mathcal{R}_{\rm R}/(1 + R_*/2r_g)$. It is shown in the Appendix that this penetration factor crucially determines the strength of tidal interaction, i.e., the amount of work the tidal forces do on the star. We show (eq. [A23]) that tidal work can be approximated by

$$W_{\rm tide} \sim G\frac{m_{\rm bh}M_*R_*^2}{r_p^3}\varepsilon^2(\beta) = M_*c^2\frac{r_g}{r_p}\frac{R_*^2}{r_p^2}\varepsilon^2(\beta), \tag{3}$$

[1] Faculty of Mathematics and Physics, University in Ljubljana, Jadranska 19, 1000 Ljubljana, Slovenia; andreja.gomboc@fmf.uni-lj.si, andrej.cadez@fmf.uni-lj.si.
[2] Also at: Astrophysics Research Institute, Liverpool John Moores University, 12 Quays House, Egerton Wharf, Birkenhead CH41 1LD, UK.

where $\varepsilon(\beta)$ can be thought of as an effective eccentricity of the star at the periastron. If the Roche radius penetration factor is large, ε may grow to values of the order of 1, bringing $W_{\rm tide}$ to values comparable to a sizeable fraction of $M_* c^2$. Thus, the tidal interaction becomes overwhelmingly strong for large β. Such an extreme scenario occurs for grazing interactions only if the size of the star is comparable to that of the black hole (see the Appendix). We classify grazing tidal interactions as follows:

1. $m_{\rm bh}/M_* \ll 1$. The Roche radius is smaller than the radius of the star; it follows that the Roche penetration factor is less than 1. As a consequence, $\varepsilon^2 \ll 1$ and the star as a whole does not suffer large perturbations, even if the black hole pierces the star and accretes a small part of its mass along the way.

2. $m_{\rm bh}/M_* \sim 1$. The Roche radius more or less equals the radius of the star (eq. [1]), and so, unless the star is very unusual, $R_* \gg r_g$, the value of the Roche penetration factor is $\beta_{\rm gr} \sim 1$. For such a $\beta_{\rm gr}$, $\varepsilon(\beta = 1) \sim 1$ (cf. the Appendix), and equation (3) predicts that the tidal energy is of the order of $10^{-5}\, M_* c^2$, which is a typical internal energy of a solar-type star. Thus, the tidal energy is just about large enough to completely distort the star; the interaction may trigger violent hydrodynamic phenomena, possibly even a supernova. The most important phenomena governing the appearance of the star during such an encounter are hydrodynamic in nature, since the strong gravity region around the black hole has a much shorter range than is the size of the perturbed star. Hydrodynamics governs the appearance of the phenomenon, and therefore, such an event does not directly reflect general relativistic effects in a strong-gravity environment.

3. $m_{\rm bh}/M_* \sim (c/v_e)^2$, where $v_e = (2GM_*/R_*)^{1/2}$ is the escape velocity from the star. The black hole radius is comparable to the size of the star; if the star is not very unusual, its escape velocity is much less than c, so according to equation (1) the Roche radius is much greater than R_* and consequently $\beta_{\rm gr} \gg 1$. In this case the tidal energy exceeds the internal energy by several orders of magnitude. A total and complete tidal disruption takes place outside the black hole but in the region sufficiently close to the black hole for relativistic effects to play the major role in the dynamics of the disruption (§ 3).

4. $(c/v_e)^2 < m_{\rm bh}/M_* < (c/v_e)^3$. The black hole radius is larger than that of the star but still smaller than the Roche radius; $\beta_{\rm gr}$ decreases with increasing mass of the black hole. The tidal energy before reaching the horizon is still comparable to the internal energy of the star. The release of tidal energy may well be sufficient to produce high-energy shocks, boosting stellar luminosity by many orders of magnitude. Yet, shocks moving with a few Mach are still much slower than the near speed of light the star is moving at now. The star remains small with respect to the black hole along its way to the black hole. Such a stellar capture will thus very closely trace relativistic effects in the spacetime, as it will be seen as a flashing point particle on its way to doom.

5. $m_{\rm bh}/M_* > (c/v_e)^3$. The black hole is very much larger in size than the star ($m_{\rm bh} > 10^8\, M_\odot$ for a solar-type star); the Roche radius lies beyond the black hole's horizon, so it follows equation (2) that the star is tidally disrupted only after crossing the horizon ($r_{\rm R} < 2r_g$). Hence, the point-particle approximation for the falling star is very good in the whole region outside the black hole. Since there is no agent to heat the star up, it is less likely for such an event to be noticed (§ 2).

Here we discuss only the last three cases, since we find them interesting as a tool to study the strong gravity regions in the universe, as well as in view of supermassive black holes in galactic nuclei.

2. STAR ENCOUNTERING A $m_{\rm bh} > 10^8\, M_\odot$ BLACK HOLE

We expect that the capture of a star by a giant black hole would most likely occur when a star in the cluster surrounding the giant black hole would be perturbed to a low angular velocity orbit with respect to the black hole. Therefore, the characteristic velocity of such encounters will most likely be that of the parabolic infall. During such an infall the star cannot be significantly disrupted while outside the horizon, so with respect to a much larger black hole it can be treated as a point source of light whose appearance with respect to the far observer will be modulated by the Doppler shift, aberration bending, and gravitational redshift. Two numerical codes were developed to calculate the apparent luminosity changes of the source falling in both Schwarzschild-type and Kerr-type black holes. During the encounter of the star with a giant black hole, the star is simulated as a point source emitting monochromatic light of frequency ν_0 and intensity L_0, both constant in the frame comoving with the source. As the source is moving along a parabolic orbit with a given orbital angular momentum, we trace light rays from subsequent points of the source's trajectory (separated by $\Delta t = 1 r_g/c$ in coordinate time) to the distant observers and calculate the apparent luminosity with respect to them as a function of time. We would like to note that these results are directly applicable also to luminosity and spectrum changes produced by orbiting blobs of material in accretion disks around black holes.

Results for both types of black holes show (Gomboc et al. 1999) two characteristic timescales of luminosity changes, both determined by the gravity of the black hole. The first one displays the basic quasi period in luminosity and redshift changes as the star spirals toward the black hole. The quasi period very closely matches the orbital period of the source at the innermost stable orbit ($50 r_g/c$ for a Schwarzschild black hole). The number of quasi periods observed depends on the fine tuning of the angular momentum to the critical value. In the Schwarzschild case the critical angular momentum is $l/M_* r_g c = \tilde{l} = 4$ and the number of quasi periods can be approximated as $N_p = 0.5 - 0.5 \log(4 - \tilde{l})$ for $3.9 < \tilde{l} < 4$. The quasi periods in the Kerr case differ for prograde and retrograde orbits: for a maximal Kerr black hole (with rotation parameter $a = 0.998 r_g$) and a star on a prograde orbit with angular momentum close to critical $\tilde{l}^+ = 2[1 + (1 - a/r_g)^{1/2}]$, the quasi period is $\approx 13 r_g/c$, while for a star on a retrograde orbit with $\tilde{l}$ close to critical $\tilde{l}^- = -2[1 + (1 + a/r_g)^{1/2}]$, the quasi period is $\approx 80 r_g/c$, both consistent with orbital periods at critical radii.

The second timescale is considerably faster (of the order of $1 r_g/c$) and belongs to the rate of change of relativistic beaming direction with respect to the observer. For the black hole with mass $m_{\rm bh} = 10^8\, M_\odot$, the corresponding timescales are $\sim$10 hr and $\sim$10 minutes, and for an extreme case of $m_{\rm bh} = 10^{10}\, M_\odot$, the time intervals are on the order of months and $\sim$10 hr. Since the luminosity and spectrum changes are caused by relativistic beaming and gravitational lensing, they are most evident to observers in the orbital plane of the star. The observers perpendicular to this plane see the source as slowly fading and then, as the source approaches the horizon, suddenly disappearing on a timescale of the order of $\sim 10 r_g/c$. Comparing results for Schwarzschild and Kerr black holes, we find that luminosity curves (Fig. 1) are qualitatively similar, but timescales generally shorten for Kerr prograde orbits and become longer for Kerr retrograde orbits. Results show that within 5° of the orbital plane one can expect luminosity to rise by a factor of a few $\times 10$, while the maximum Doppler plus redshift factor ($\nu_{\rm obs}/\nu_0$) is 1.8 for

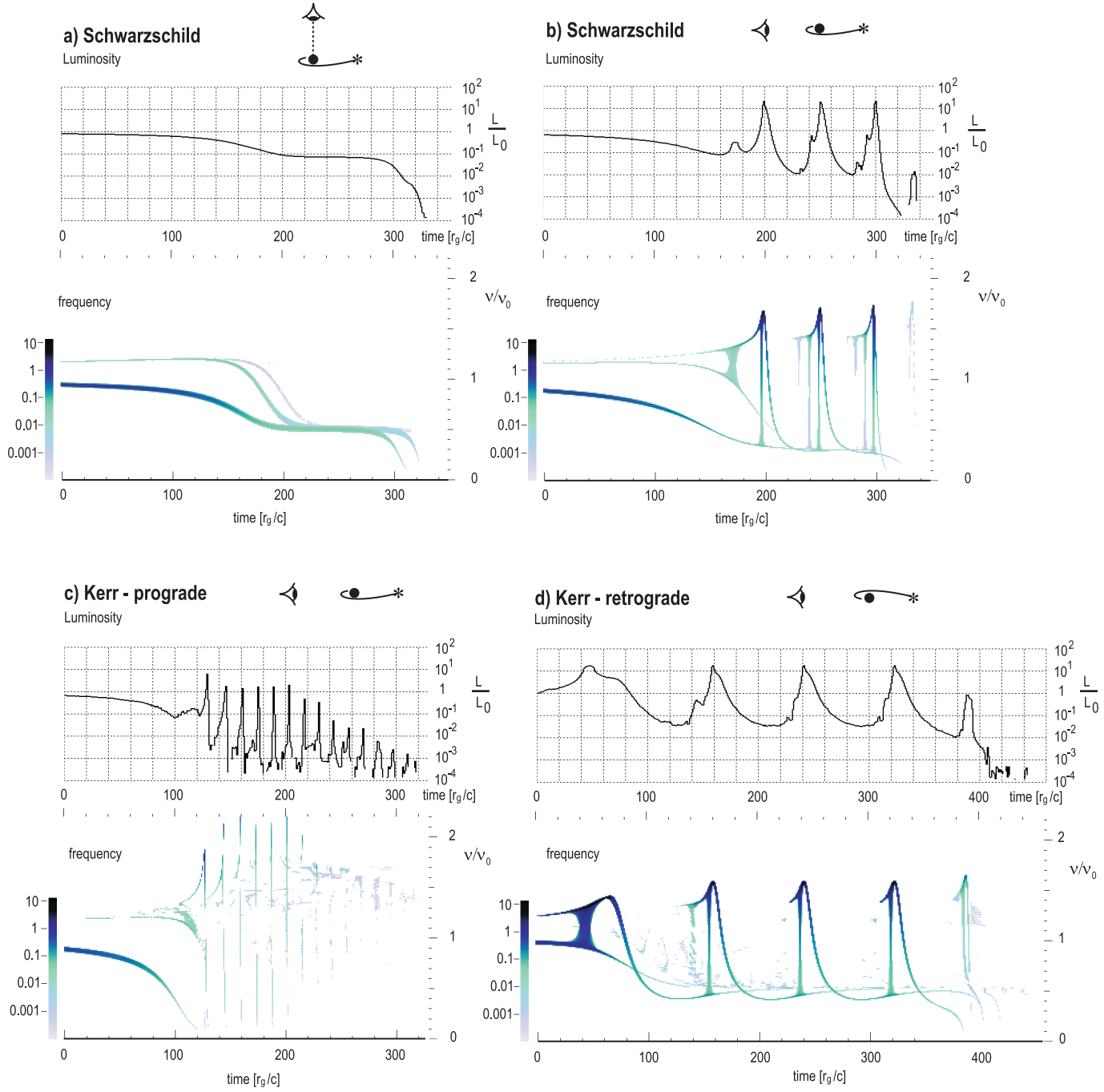

FIG. 1.—Luminosity and frequency shift during the infall of a solar-type star into a giant black hole $m_{\rm bh} > 10^8\ M_\odot$. (*a*) Infall with orbital angular momentum $\tilde{l}$ close to the critical $\tilde{l} = 4$ value into the Schwarzschild black hole, as observed perpendicular to the orbital plane. (*b*) Same event observed in the orbital plane. (*c*) Infall of the star on a prograde orbit with $\tilde{l}$ close to the critical $\tilde{l}^+$ value into the Kerr black hole, as observed in the orbital plane. (*d*) Infall of the star on a retrograde orbit with $\tilde{l}$ close to the critical $\tilde{l}^-$ value into the Kerr black hole, as observed in the orbital plane. The color code in the frequency diagram corresponds to spectrum intensity (in units of the initial intensity of the primary image).

the Schwarzschild case and 2.2 for the maximal Kerr black hole case.

3. STAR ENCOUNTERING A $m_{\rm bh} \sim 10^5$–$10^6\ M_\odot$ BLACK HOLE

3.1. *Approximations, Model, and Comparison with Hydrodynamic Results*

The capture of a star by a black hole of comparable size is a phenomenon in which a black hole's gravity plays the dominating role both on the propagation of light as well as on the propagation of matter belonging to the star. This property of the phenomenon is forcefully stressed by the fact that the tidal energy is many orders of magnitude larger than its gravitational binding energy and becomes a sizeable fraction of $M_* c^2$ (eq. [3]). Therefore, we build our approach on the work of Luminet & Marck (1985), who showed that in the vicinity of the black hole, "particles of the star undergo a phase of approximate free fall in the external gravitational field, since the tidal contribution grows much larger than pressure and self gravitating terms." Therefore,

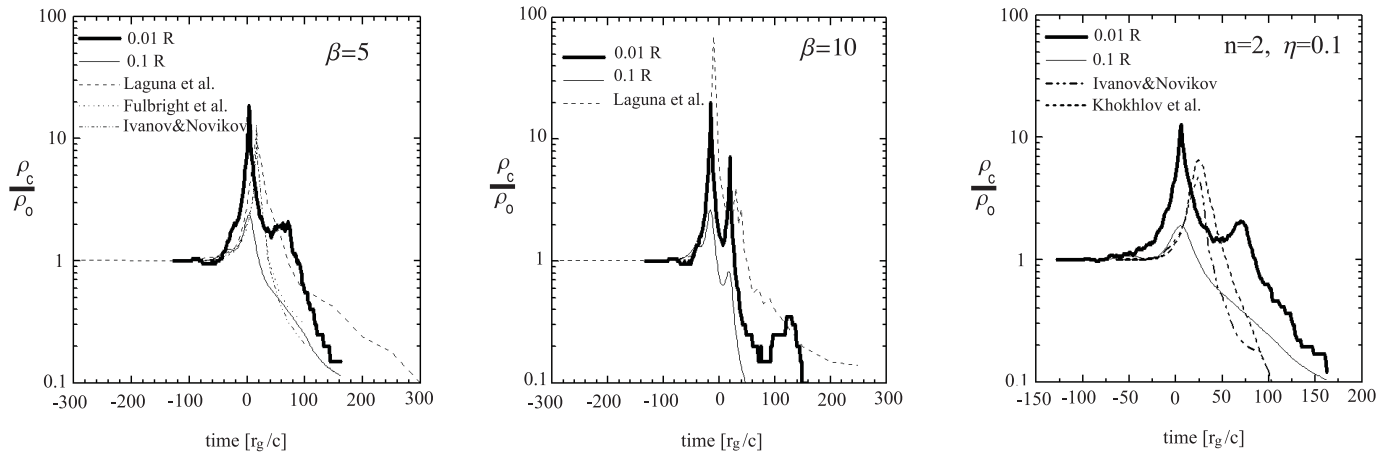

FIG. 2.—Central density in the star as a function of time during a close encounter for polytrope $n = 1.5$: $\beta = 5$ ($\tilde{l} = 5$), $\beta = 10$ ($\tilde{l} = 4.08$), and $n = 2$, $\eta = 0.1$ [$\eta = (M_*/m_{\rm bh})^{1/2}(r_p/R_*)^{3/2}$]. Solid curves are from our simulations, dashed are from Laguna et al. (1993), dotted from Fulbright et al. (1995), dot-dashed from Ivanov & Novikov (2001), and short-dashed from Khokhlov et al. (1993b). Time is measured from the periastron passage.

we use a simple model, whereby the star is considered as undisturbed by the black hole (i.e., spherically symmetric) until it reaches the Roche radius. After crossing it, the black hole's gravity takes over and the self-gravity and internal pressure are completely switched off.

In addition, we neglect hydrodynamic effects. This approximation is justified if the proper time elapsed between the Roche radius crossing and total disruption is short compared to the dynamic timescale τ_d of the star. For an estimate of the two timescales, we take

$$\tau_d = \left(\frac{G\varrho_*}{3\pi}\right)^{-1/2}, \tag{4}$$

$$\tau_{\rm R} \sim \frac{\sqrt{2}}{3c} r_g \mathcal{R}_R^{3/2} = (6\pi G\varrho_*)^{-1/2}, \tag{5}$$

where $\tau_{\rm R}$ is estimated as the proper time elapsed during a radial parabolic infall from the Roche radius to the horizon.[3] Specifically, for a solar-type star we obtain $\tau_{\rm R} \sim 13$ minutes, which is an order of magnitude less than the dynamic timescale $\tau_d \approx 3$ hr. The ratio of the two times indicates that the amount of energy exchanged may not be quite negligible but is small enough that it may be neglected in the first approximation. Further justification for such an approximation comes from results of hydrodynamic evolution calculated by Kochanek (1994) and Laguna et al. (1993). Laguna et al. noted that "the qualitative features of the debris—including its crescent-like shape—can be reproduced by neglecting the hydrodynamic interactions and self-gravity of the star," since the formation of the crescent is due to "geodesic motion of the fluid elements of the star in a Schwarzschild spacetime which includes the relativistic-induced precession of the orbit about the black hole." This confirms previously mentioned findings by Luminet & Marck (1985) that a black hole's gravity dominates in close encounters. Therefore, we argue that by neglecting hydrodynamic effects, we obtain in close encounters approximately the correct shape of stellar debris.

Hence, our numerical model starts with a spherically symmetric star of radius R_* and mass M_* consisting of N equally massive constituents ($m_i = M_*/N$, $N \sim 10^6$) distributed randomly but in such a way that, on average, their density distribution follows that of a star, which is approximated by the polytrope model with $n = 1.5$. All constituents of the star start with the (same) velocity, corresponding to the parabolic velocity of the star's center of mass, which is placed at a distance $\mathcal{R}_{\rm R}$ from the black hole. Subsequently, the positions of free-falling stellar constituents are calculated at later discrete times (t_i) according to general relativistic equations of motion.

To test the errors induced by these approximations, we study encounters of a solar mass, solar radius star with a $10^6\,M_\odot$ black hole and compare our results on central density in the star (average density inside $0.01R_*$) with those obtained by Laguna et al. (1993), Fulbright et al. (1995), Khokhlov et al. (1993b), and Ivanov & Novikov (2001). Figure 2 shows the central density as a function of time with respect to the time of periastron passage as obtained by our model and by hydrodynamic simulations. The qualitative agreement between these results justifies the neglect of internal pressure in calculating the dynamics of disruption. The major difference seems to be in the precise timing of tidal compression: in our model the strongest compression occurs very close to periastron, in agreement with the results of Luminet & Marck (1985), while in most hydrodynamics simulations the central density peaks approximately $(15–20)r_g/c$ after the periastron passage.

Our results on the shape of stellar debris during the close encounter also agree with results of Laguna et al. (1993), although at later times our crescent becomes considerably longer.

3.2. *On the Luminosity of the Star during the Tidal Disruption*

We consider the tidal disruption to be the phenomenon in which the work done on the star by tidal forces is comparable or greater than its initial internal energy. The tidal disruption is thus a violent nonstationary process that takes place in the vicinity of the black hole on a timescale that is considerably shorter than the stellar dynamic timescale (measured in proper time of the falling star). As the star is deformed into a long thread, the giant tidal wave deposits great amounts of energy that soon pushes gases into an outward-moving shock wave more or less perpendicular to the threadlike axis of the star. Thus, during the disruption process several mechanisms play an important role: shocks, adiabatic expansion, and cooling of disrupted material, possible explosions due to tidal squeezings as predicted by Carter & Luminet (1982, 1985),

[3] Of course, $\tau_{\rm R}$ is defined only for $r_{\rm R} > 2r_g$, when tidal disruption takes place outside the horizon of the black hole. For nonzero angular momentum orbits, $\tau_{\rm R}$ is slightly but not crucially longer.

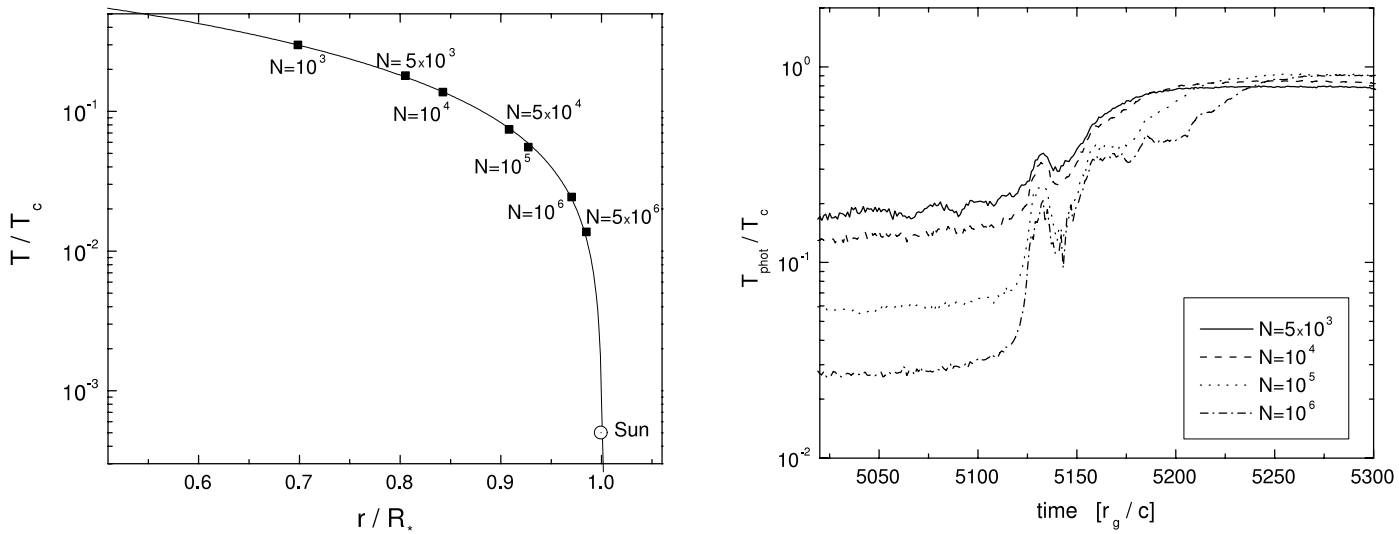

FIG. 3.—*Left*: Model atmosphere depth in the initial (spherically symmetric) star: polytrope temperature profile (*line*) and photospheric temperatures and corresponding depths for different N in our model (*symbols*). *Right*: Photospheric temperature as a function of time during total tidal disruption given by our model for different N.

radiation driven expansion, etc. These effects have no doubt important influence on the cooling and luminosity of the disrupted star, but we wish to stress that, as shown by Luminet & Marck (1985), gravity in general overwhelms other forces during the close encounter. So, since gravity of the black hole swings the star around on a timescale that is much shorter than any other timescale that may play a role, we believe that, as a first step to estimate the luminosity variations of the tidally disrupted star, we may use a simple model, which must in the first place correctly take into account the effects of the dominating strong gravitational field of the black hole. As the disruption progresses and the hot stellar inner layers become exposed both by gravity and by shock waves, the luminosity is bound to rise because of the higher effective temperature and because of the higher effective area seen. The overall rise in luminosity depends on other partially competing mechanisms involved: while the expansion and cooling would tend to reduce it, it must nevertheless rise dramatically because of enormous work being done by tidal forces that drive shock heating and supernova-like explosions. The precise role of these mechanisms and their influence on stellar structure and evolution need detailed analysis but is beyond the scope of this paper.

Here we wish to take a step toward the complete solution by including in full only the most important ingredient defining the shortest timescales: the effects of a black hole's gravity on the apparent variability of stellar luminosity. The standard stellar atmosphere model (Bowers & Deeming 1984; Carroll & Ostlie 1996; Swihart 1971) is not applicable in calculating the effective temperature of any surface element, since, because of the highly dynamic structure, the fine details of atmospheric density, temperature, and pressure profiles are not available; even more, we cannot predict in advance which part of the star is going to, at some future time, belong to the atmosphere. So we are forced to apply a Monte Carlo model throughout the star by which the unperturbed star is modeled as a spherical cloud consisting of a large number (N) of identical constituents distributed randomly but in such a way that their average density follows that of an $n = 1.5$ polytropic model (cf. § 3.1). The constituents are optically thick and have an assigned temperature according to their position in the cloud, which again follows the temperature profile of the $n = 1.5$ polytropic stellar model. The model photospheric temperature and model luminosity are calculated as the sum of spectral contributions from those cloud constituents that are seen by the observer, i.e., by those that are not obscured by constituents in overlaying layers. For the purpose of obscuration, all the constituents are considered to have the same cross section σ, so that $\sigma = 4\pi R_*^2/N'$, where the parameter N' is the number of constituents belonging to the "atmosphere" of the star. It is clear that, since for statistical reasons N' must be at least a few tens, and N is limited by the computer power to a few million, the ratio N'/N is much greater than the ratio $M_{\rm atm}/M_*$ in a real star. One could argue that the atmosphere could be made less massive by representing it with a larger number of less massive constituents. However, in the case of total tidal disruption the interior is mixed into the atmosphere during the late stages of disruption, and the so-introduced uneven opacity of stellar constituents would further complicate the interpretation of results. Thus, we cannot afford to make models with sufficiently opaque atmospheres, and as a result, our initial model photospheric temperatures are too high. We note, however, that the model photospheric depth is a function of N'/N, so by changing N, we probe the stellar atmosphere to different depths. In such a way an extrapolation to realistic opacities is possible. The consistency of such an extrapolation is checked on the initial spherically symmetric stellar model, in which the Monte Carlo results can be directly compared with the theoretical atmospheric model. An example of such a comparison is shown in Figure 3. It is clear that the depth of our model photospheres is some orders of magnitude too high, yet it is possible to extrapolate model photospheres to depths of realistic stellar atmospheres, since the temperature is a monotonic smooth function of depth. For evolved stages of tidal disruption there is no underlying theoretical model, so we rely on extrapolated results of the Monte Carlo model.

As the star moves along the orbit, images of the star with respect to the far observer are formed as follows. Photon trajectories and the time of flight between each stellar constituent and the observer are calculated with a technique described in Čadež et al. (2003), Gomboc (2001), Brajnik (1999), and Čadež & Gomboc (1996). Only two trajectories connecting two space points are considered, the shortest one and the one passing the black hole on the other side, while those winding around the

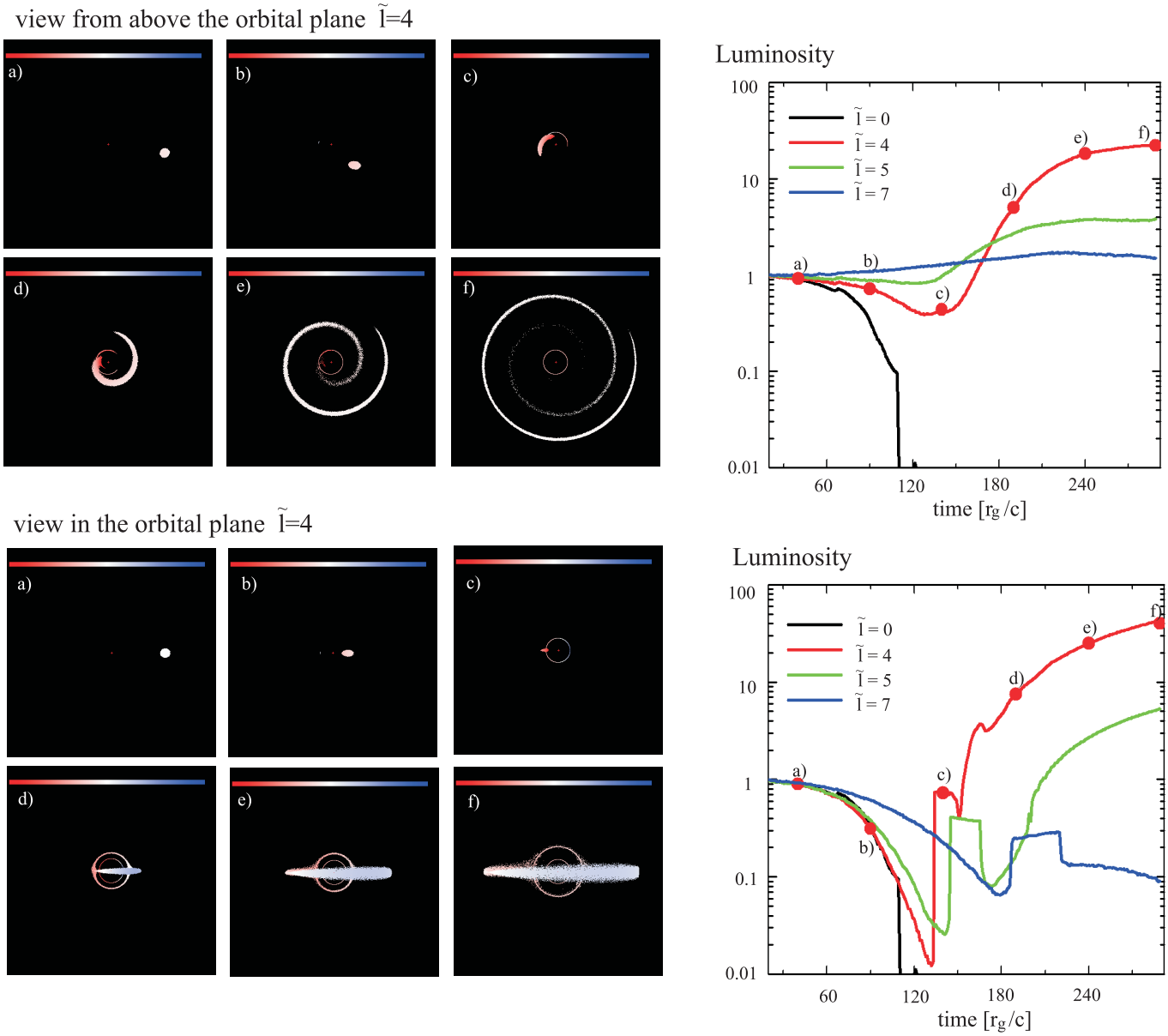

FIG. 4.—Isothermal star with $R_* = 2r_g$ during the encounter with the critical $\tilde{l} = 4$ value. The top panels are for the observer perpendicular to the orbital plane and the bottom panels are for the observer in the orbital plane. Pictures show the stellar appearance at time intervals of $50r_g/c$, with color corresponding to the apparent temperature: gravitational redshift close to the black hole and Doppler shift of receding material stretch the observed frequency of photons (and therefore the observed temperature of the stellar surface) toward zero (*red*), while the Doppler shift of approaching material increases the observed temperature (*blue*, corresponding to the value of twice the temperature in the system comoving with the star). Graphs show the apparent luminosity at different stages of the encounter (in units of the stellar luminosity before the encounter) and for different orbital angular momenta $\tilde{l} = 0$, 4, 5, and 7.

black hole by more than 2π are neglected. (It has been shown before [Čadež & Gomboc 1996] that light following trajectories with higher winding numbers contributes less and less to the apparent luminosity.) The beam contributions are sorted into pixels with an area corresponding to the size of σ and tagged according to the arrival time. The intensity corresponding to a given pixel is then defined as the intensity corresponding to the ray with the shortest travel time. Since light from deeper layers takes longer to reach the observer, this takes care of the obscuration of deep layers. The intensity of a contributing beam is calculated assuming that the corresponding stellar constituent emits in its own rest frame as a blackbody at its temperature. The apparent luminosity and effective temperature of the star as a function of time (with respect to the chosen observer) are calculated and successive stellar images, formed in this way, are pasted into a movie.[4]

We divide our model into three parts. First we estimate the relativistic effects alone by simulating the luminosity variations of an isothermal star [i.e., a star with $T(r, t) = \text{const.}$]. In the next step, we consider the star with a polytrope $n = 1.5$ temperature profile and estimate the luminosity variations due to the exposure of inner hot regions of the star. We first consider a simple case, in which the temperature of all stellar constituents is constant in time (no cooling or heating), and afterward add a rough estimation of the effect of cooling of the exposed stellar parts on the stellar luminosity.

[4] Movies can be obtained at http://www.fmf.uni-lj.si/~gomboc.

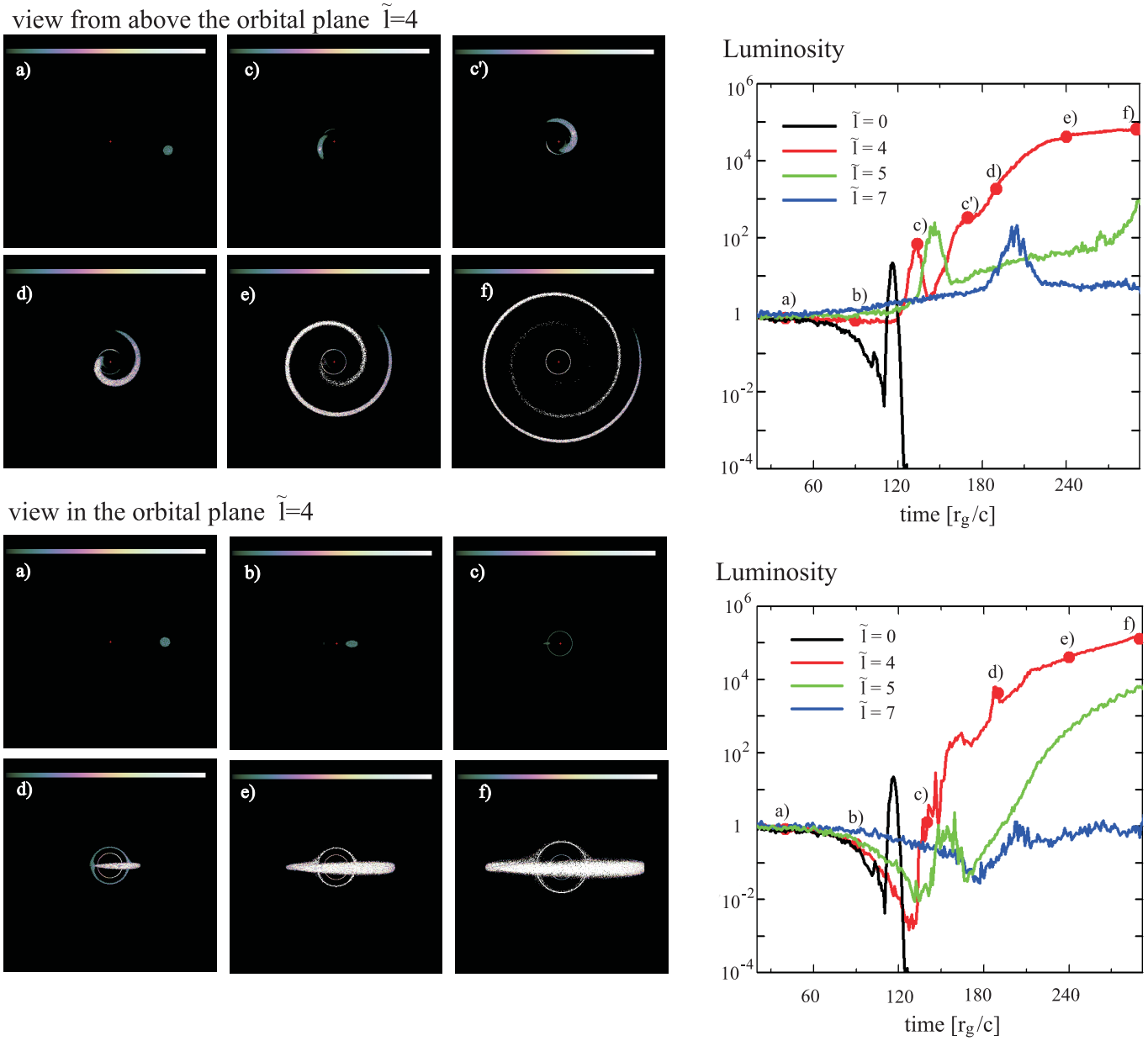

FIG. 5.—Star with $R_* = 2r_g$ and $\tilde{l} = 4$ during the encounter assuming no temperature change of the debris. Pictures show the stellar appearance at time intervals of $50r_g/c$ (except c and c', see graph) with color corresponding to the apparent temperature according to the color code: blue, temperature zero; white, $0.5T_c$ or higher. Inset graph shows the apparent luminosity at different stages of the encounter (in units of the initial luminosity far from the black hole) and for different orbital angular momenta $\tilde{l} = 0$, 4, 5, and 7. The top panels are for the observer perpendicular to the orbital plane, and the bottom panels are for the observer in the orbital plane.

3.2.1. *Effects of a Black Hole's Gravity*

To isolate the effect of gravity, we first compute luminosity variations of an isothermal star. The ensuing luminosity variations can be ascribed to Doppler boosting and aberration of light, gravitational lensing and redshift (similar to that for a pointlike source in § 2), and the elongation of the star due to relativistic precession and due to tidal squeezing. Figure 4 shows the obtained luminosity variations as a function of time for encounters with $\tilde{l} = 0$ (radial infall), $\tilde{l} = 4$ (critical), $\tilde{l} = 5$ ($r_p = 10r_g$), and $\tilde{l} = 7$ ($r_p = 22.3r_g$) as seen perpendicular to and *in* the orbital plane.

Results show that the maximal rise in luminosity occurs in the case of the critical encounter ($\tilde{l} = 4$), in which the overall luminosity rise due to the elongation of the star is of a factor of about 20 (as seen by the observer perpendicular to the orbital plane; Fig. 4, *top*), while gravitational lensing and Doppler boosting enhance it up to about 40 times the initial luminosity (Fig. 4, *bottom*). Observers close to the orbital plane see the most extreme variations: dimming of the receding star, its rebrightening as it emerges from behind the black hole, and variations on short timescales of about $10r_g/c$, which are due to lensing effects. Since the star and the black hole are comparable in size, the probability that they are aligned with respect to the observer is high. When lensing takes place, the relevant part of the star is imaged into an Einstein disk and the apparent luminosity increases manifold (Fig. 4*c*).

3.2.2. *Constant Temperature Debris*

Next, we consider the star with an $n = 1.5$ polytrope temperature profile, and we assume that the temperature of stellar debris does not change with time. The model is obviously much

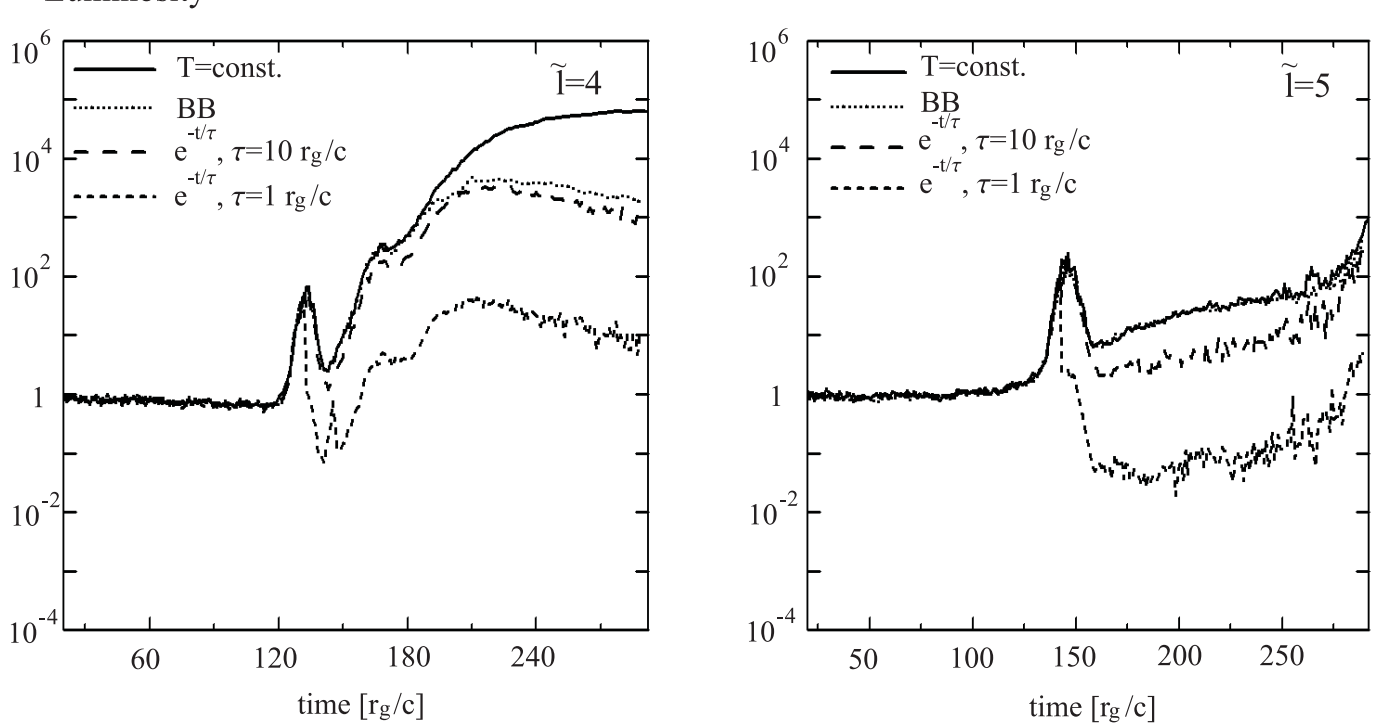

FIG. 6.—Effect of the cooling of the debris on the luminosity variations: solid line, no cooling; dotted, cooling by blackbody radiation; dashed lines, exponential cooling with decaying time $10r_g/c$ (*long-dashed*) and $1r_g/c$ (*short-dashed*). Results are for the star on the $\tilde{l} = 4$ (*left*) and $\tilde{l} = 5$ (*right*) orbits as observed perpendicular to the orbital plane.

too crude to rely upon its results regarding the spectral characteristics or even the absolute value of the emitted luminosity. The crude argument why this model may bear some resemblance to the true light curve is that a shock wave released by the unbalance of gravity carries internal energy to the surface in such a way that the energy influx from the interior temporarily compensates the radiation loss.

The simulation shows that, as the inner hot layers of the star are exposed during the disruption, they contribute to the substantial rise in stellar luminosity, depending on the orbital angular momentum of the star (Fig. 5). The star on a low angular momentum orbit is completely captured by the black hole and produces only a short $[\sim(1-10)r_g/c]$ flare before disappearing behind the horizon. On the other hand, the star with high angular momentum experiences only a slight distortion during the distant flyby, with a resulting temporary $[\sim(10-100)r_g/c]$ slight increase in luminosity.

The most dramatic effect occurs when the star is on the critical angular momentum orbit ($\tilde{l} = 4$). During such an encounter half of the stellar constituents are swallowed by the black hole and the other half escape. During this process, the star is totally tidally disrupted in such a way that the higher angular momentum material rapidly lags behind the stellar debris with lower angular momentum, which produces a long, thin spiral (Fig. 5). Outer layers of the star are stripped off in a time of the order of $100r_g/c$, the depth to the hot inner core decreasing together with self-gravity. In our crude model this is seen as decreasing optical thickness and the exposure of the hot inner core; the luminosity rises steeply. The spectrum of the debris is dominated by the emission of the innermost exposed layers, and as long as shock waves are building up, i.e., until cooling sets in, these lead to X-rays.

Some luminosity peaks arise from the effect of tidal compression in the direction perpendicular to the orbital plane of the star, which in our model for a short time exposes the interior of the star. Such peaks are evident in Figure 5 (*top*, *c* and *c′*), and these two compressions are in agreement with multiple tidal squeezings predicted by Luminet & Marck (1985) and confirmed by Laguna et al. (1993). In our model they produce luminosity peaks lasting $\approx 5r_g/c$. As mentioned earlier, Carter & Luminet (1982, 1985) predict that a thermonuclear explosion may occur at this moment.

The scale of the luminosity rise in Figure 5 is rather uncertain due to the neglect of hydrodynamic effects[5] and also due to our poor atmospheric model (§ 3.2). For the critical tidal disruption of the Sun, the extrapolation of our model would suggest the total luminosity to rise to about $10^{13}\ L_\odot$ (mostly in X-rays), which accentuates the extent of tidal disruption but also sends a warning that by that time our constant internal energy model assumption ceases to be valid. As suggested in § 3.2, we calculated a range of models with N between 10^3 and 10^6 and extrapolated the results to realistic atmospheric depths. These numerical results suggest that, at least for the critical disruption, the average temperature and size of the final crescent to which the star is deformed is roughly independent of N. Thus, we tested the idea that tidal disruption exposes or mixes up by shearing the envelope of the star to a certain depth R_c, which we define as the depth in the undisturbed star down to which the average T^4 is equal to the average T^4 of the final crescent. In this way we estimate (independent of N) that for critical $\tilde{l} = 4$ and $n = 1.5$, R_c is about $0.25R_*$, while for $n = 5$ we get $R_c = 0.1R_*$. For a close flyby with $\tilde{l} = 5$, R_c is about $0.7R_*$ and $0.5R_*$ for $n = 1.5$ and 5, respectively. We may also, as an example, estimate

[5] For simplicity, we assume that all the tidal energy is transformed into the kinetic energy of the tidal wave; the portion of kinetic energy that may go into heat is neglected, and therefore, we expect that the actual available luminous energy during such a tidal disruption may be higher than the one given by our models.

the luminosity of a solar-type star during the bright critical stage of total disruption on a $10^6\ M_\odot$ black hole as follows: the steep luminosity rise (cf. Fig. 5) has a timescale between $30r_g/c$ and $100r_g/c$, which is about 2.5–8 minutes. Assuming that the initial thermal energy contained in the exposed layers ($\sim 10^{48}$ ergs) is radiated away on this timescale, the critical luminosity would be of the order of $(5-15)\times 10^{11}\ L_\odot$.

After the debris is spread and starts moving away from the black hole, the physics of tidal disruption is no longer dominated by the black hole's gravity. The physical conditions in stellar debris, the physics of radiation processes, magnetohydrodynamics, take over, and the ensuing processes go beyond the simulation presented here.

3.2.3. *Cooling of Stellar Debris*

In general, the temperature inside the star may change due to various mechanisms already mentioned. To get an idea of how they might affect the light curve, we again model the cooling in two very approximative ways:

1. exponential cooling of exposed stellar layers with different characteristic times: $\tau = 1r_g/c$ and $10r_g/c$,
2. cooling of exposed stellar layers due to their own blackbody radiation in the 4π solid angle.

Results presented in Figure 6 show that if the cooling were very efficient, with timescales of $1r_g/c$, the luminosity rise would be quite short and modest.

4. CONCLUSION

A stellar encounter with a massive black hole can be a very energetic event, with energy released and luminosity variations depending primarily on the relative size of the star compared to the black hole. We note that the tidal interaction energy may rise to as high as 10% of the total mass-energy of the captured star, which is available when the star is comparable in size to the size of the black hole. This size ratio is also critical to the nature of the disruption.

In this work we focused on gravitational phenomena and showed that:

1. A critical capture of a "pointlike star" is characterized by a series of quasi-periodic apparent luminosity peaks with the quasi period $50r_g/c$ for a Schwarzschild black hole and $13r_g/c$ and $80r_g/c$ for an extreme Kerr co- and counterrotating case, respectively (Fig. 1). This translates into $(6.9\ \mathrm{hr})m_{\mathrm{bh}}/(10^8\ M_\odot)$, $(1.8\ \mathrm{hr})m_{\mathrm{bh}}/(10^8\ M_\odot)$, and $(11.1\ \mathrm{hr})m_{\mathrm{bh}}/(10^8\ M_\odot)$, respectively. If a pointlike star were a planet falling toward a $3.6\times 10^6\ M_\odot$ black hole in the Galactic center, respective quasi periods would be 15, 3.9, and 24 minutes.
2. The sharpness, the amplitude of quasi-periodic peaks, and the amplitude of the Doppler factor are more pronounced for observers in the orbital plane as compared to those perpendicular to this plane. The highest value for the Doppler factor is 1.8 for the Schwarzschild and 2.2 for the extreme Kerr black hole.
3. The number of quasi-periodic peaks (N_p) depends on the closeness of the orbital angular momentum ($\tilde{l}$) to the critical value $\tilde{l} = 4$ and can be approximated as $N_p = 0.5 - 0.5\log(4-\tilde{l})$.
4. An extended star may be approximated as a collection of point particles when heading toward the complete tidal disruption. The shape and the density of the debris calculated in this approximation compare well with more sophisticated hydrodynamic calculations (cf. § 3).
5. Model light curves for critical tidal disruption of a star of the same size as that of the black hole (Figs. 4, 5, and 6) calculated for different heuristic models show similar temporal characteristics that display very rapid (on a timescale of the order of $10r_g/c$) luminosity variations by a few or even many orders of magnitude, while the quasi periodicity is no longer pronounced in such a process. Light curves describing a critical capture are very rough and cannot be momentarily calibrated in flux. They are presented as they produce the extremely short timescale phenomena characteristic of the strength of a black hole's gravitational field. We also believe that the main characteristics of tidal disruption as expressed by this rather crude model will be recognizable also in more elaborate future models of tidal disruption.

We thank the anonymous referee for constructive criticism, which helped us improve the text. We acknowledge the financial support of the Slovenian Ministry of Science, Education and Sport. A. G. also acknowledges the receipt of the Marie Curie Fellowship from the European Commission.

APPENDIX

THE VIRIAL THEOREM AND TIDAL ENERGY

In order to estimate the amount of heat and kinetic energy deposited to the star by the tidal wave, it is useful to follow the steps of the derivation of the virial theorem. Consider the some 10^{57} nuclei and electrons making up the star as representative point particles making up the ideal gas of the star. Each of the particles with mass m_i (where $i = 1. \ . \ .10^{57}$) moves according to Newton's law (we follow the more transparent classical derivation, which is sufficient for order-of-magnitude arguments):

$$m_i\ddot{\boldsymbol{r}}_i = \sum_{j\neq i}\boldsymbol{F}^c_{ij} + \sum_{j\neq i} G\frac{m_i m_j}{\left|\boldsymbol{r}_j-\boldsymbol{r}_i\right|^3}\left(\boldsymbol{r}_j-\boldsymbol{r}_i\right) - G\frac{m_{\mathrm{bh}}m_i}{r_i^3}\boldsymbol{r}_i. \tag{A1}$$

The black hole has been placed at the origin from where the position vectors $\boldsymbol{r}_i$ are reconed. The vector $\boldsymbol{F}^c_{ij}$ models the force taking place during particle collisions. It obeys (the strong version of) Newton's third law, and since in the ideal gas approximation collisional forces act only at a point, the energy connected with the potential of these forces can be neglected. The second term on the right describes the gravitational interaction among the constituents of the star, and the last term represents the gravitational force of the black hole. It is convenient to define the center-of-mass position vector $\boldsymbol{R} = (\sum_i m_i\boldsymbol{r}_i)/M_*$, so $\boldsymbol{r}_i = \boldsymbol{R} + \boldsymbol{r}'_i$ and $\sum_i m_i\boldsymbol{r}'_i = 0$. Summing equation (A1) over all i, one obtains the center-of-mass equation of motion in the form

$$M_*\ddot{\boldsymbol{R}} = -G\frac{m_{\mathrm{bh}}M_*}{R^3}\boldsymbol{R} - 5Gm_{\mathrm{bh}}\frac{\boldsymbol{R}\cdot\mathbf{Q}\cdot\boldsymbol{R}}{R^7}\boldsymbol{R} + 2Gm_{\mathrm{bh}}\frac{\mathbf{Q}\cdot\boldsymbol{R}}{R^5} + \mathcal{O}(1/R^5), \tag{A2}$$

where **Q** is the quadrupole moment tensor of the mass distribution with respect to the center of mass of the star defined in the usual way as

$$\mathbf{Q} = \frac{1}{2}\sum_i m_i\left(3\boldsymbol{r}_i\boldsymbol{r}_i - \mathbf{I}\, r_i^2\right). \tag{A3}$$

Terms of $\mathcal{O}(1/R^5)$ and higher will henceforth be neglected. If the star is deformed in a prolate ellipsoid with the long axis in the direction $\hat{\boldsymbol{n}}$, **Q** can be written in the form

$$\mathbf{Q} = 3q\hat{\boldsymbol{n}}\hat{\boldsymbol{n}} - q\mathbf{I}, \tag{A4}$$

with q being positive and proportional to the eccentricity of the ellipsoid. Here $\boldsymbol{r}_i\boldsymbol{r}_i$ stands for the dyadic product of the respective vectors, and **I** is the identity matrix.

The angular momentum of the star ($\boldsymbol{l}$), which is a conserved quantity, can be split into the orbital ($\boldsymbol{l}_o = M\boldsymbol{R}\times\dot{\boldsymbol{R}}$) and spin part ($\boldsymbol{l}_s = \sum_i m_i\boldsymbol{r}_i'\times\dot{\boldsymbol{r}}_i'$). The time derivative of the orbital part follows from equation (A2), and when equation (A4) applies, it can be written as

$$\dot{\boldsymbol{l}}_o = 6G\frac{m_{\rm bh}q}{R^5}(\boldsymbol{R}\times\hat{\boldsymbol{n}})(\boldsymbol{R}\cdot\hat{\boldsymbol{n}}). \tag{A5}$$

The sum of scalar products of equation (A1) by $\dot{\boldsymbol{r}}_i$ gives the energy conservation law. We split the kinetic energy of the star into the center-of-mass part $(M_*\dot{\boldsymbol{R}}^2)/2$ and the internal kinetic energy part[6] $W_{\rm int} = \sum_i[(m_i\dot{\boldsymbol{r}}_i^2)/2]$. Using equation (A2) and neglecting the collisional interaction energy, we obtain the conserved energy E in the following form:

$$E = \frac{1}{2}M_*\dot{\boldsymbol{R}}^2 - G\frac{m_{\rm bh}M_*}{R} - G\frac{m_{\rm bh}\boldsymbol{R}\cdot\mathbf{Q}\cdot\boldsymbol{R}}{R^5} + W_{\rm int} + W_G, \tag{A6}$$

where W_G is the self-gravitational energy of the star [$W_G = (-1/2)\sum_i\sum_{j\neq i}G(m_im_j/|\boldsymbol{r}_j - \boldsymbol{r}_i|)$].

Finally, we obtain the equivalent of the virial theorem by multiplying equation (A1) by $\boldsymbol{r}_i'$ and summing over all i. The result can be rearranged into the transparent form

$$W_{\rm int} + \frac{1}{2}W_G = -G\frac{m_{\rm bh}\boldsymbol{R}\cdot\mathbf{Q}\cdot\boldsymbol{R}}{R^5} + \frac{1}{4}\ddot{J}, \tag{A7}$$

where $J = \sum_i m_i r_i'^2$. For a star in hydrostatic equilibrium, the right side vanishes and the total energy of the star $W_{\rm tot} = W_{\rm int} + W_G = -W_{\rm int}$. If the star is not in hydrostatic equilibrium, the right side of equation (A7) can be considered as the energy imbalance; if it is more than $W_{\rm int}$, it is sufficient to completely disrupt the star on a timescale τ_d. An exact evaluation of this energy imbalance is beyond reach in this simple analysis; however, a simplified model offers some clues.

Consider an idealized case of an "incompressible star" flying about a massive black hole. From the point of view of the star, gravity is exerting a tidal force, squeezing it in the plane defined by the temporary radius vector and the orbital angular momentum and elongating it perpendicular to this plane. The tidal force acts to accelerate the surface of the star with respect to the center of mass, but it must also act against rising pressure and internal gravity. Thus, roughly speaking, the tidal force does work in pumping kinetic energy into the tidal wave but also in loading the gravitational potential energy that acts as the spring energy driving oscillation modes of the star. Consider small tidal distortions. In this case quadrupole deformations are dominant, so the deformation field ($\boldsymbol{U}$) of the incompressible star can be described as a linear combination of five degenerate quadrupole modes:

$$\boldsymbol{U} = \sum_{k=1}^{5} a_k\boldsymbol{\mathcal{U}}_k. \tag{A8}$$

Here $\boldsymbol{\mathcal{U}}_k$ are modal base vector fields that can be expressed as gradients of quadratic polynomials in coordinates x', y', z', obtained by multiplying spherical functions $Y_{2m}(\theta', \phi')$ by r'^2 and identifying $x' = r'\sin\theta'\cos\phi'$, $y' = r'\sin\theta'\sin\phi'$, $z' = r'\cos\theta'$, and $a_k(t)$ are modal amplitudes. In the coordinate system in which the z' axis is normal to the orbital plane and x' points from the periastron to the black hole, only three amplitudes are excited and the corresponding modal base fields are

$$\boldsymbol{\mathcal{U}}_5 = -\sqrt{\frac{5}{4\pi}}(-x, -y, 2z), \quad \boldsymbol{\mathcal{U}}_1 = -\sqrt{\frac{15}{4\pi}}(x, -y, 0), \quad \boldsymbol{\mathcal{U}}_2 = -\sqrt{\frac{15}{4\pi}}(y, x, 0). \tag{A9}$$

[6] Note that $W_{\rm int}$ comprises both the kinetic energy of thermal motion and the kinetic energy of bulk motion in the tidal wave.

These deformations lead to the following quadrupole moments:

$$\mathbf{Q} = \frac{1}{4\pi}\begin{bmatrix} a_1^2 + a_2^2 - 2\sqrt{3}a_1a_5 - a_5^2, -2\sqrt{3}a_2a_5, 0 \\ -2\sqrt{3}a_2a_5, a_1^2 + a_2^2 + 2\sqrt{3}a_1a_5 - a_5^2, 0 \\ 0, 0, -2\left(a_1^2 + a_2^2 - a_5^2\right) \end{bmatrix}. \tag{A10}$$

As long as tidal modes can be considered roughly independent, their dynamics can be derived from the Lagrange function $L = T - U$ with the kinetic energy (T)

$$T = \sum_{k=1}^{5}\sum_{l=1}^{5}\int \rho \dot{a}_k\dot{a}_l \boldsymbol{\mathcal{U}}_k \cdot \boldsymbol{\mathcal{U}}_l \, dV' = \frac{3}{4\pi}M_*R_*^2\sum_{i=1}^{5}\dot{a}_i^2 \tag{A11}$$

and the potential energy (U, the deviation of self-gravity from the equilibrium value in undeformed state)

$$U = \frac{3}{4\pi}M_*R_*^2\sum_{i=1}^{5}\omega_q^2 a_i^2, \tag{A12}$$

where ω_q is the resonant frequency of quadrupole modes. For a star consisting of a self-gravitating incompressible fluid, we obtain

$$\omega_q^2 = \frac{64}{5}GM_*/R_*^3. \tag{A13}$$

Generalized forces exciting these modes are (Goldstein 1981)

$$F_k = \int \rho G\frac{m_{\rm bh}}{R^3}\boldsymbol{\mathcal{U}}_k \cdot \left(\mathbf{I} - 3\frac{\boldsymbol{R}}{R}\frac{\boldsymbol{R}}{R}\right)\cdot \boldsymbol{r}' \, dV'. \tag{A14}$$

Let us calculate these forces in the specific case when one can assume that $\boldsymbol{R}(t)$ represents a parabolic orbit. We express the components of $\boldsymbol{R}$ as

$$\boldsymbol{R}(t) = R(t)[\cos\psi(t), \sin\psi(t), 0], \tag{A15}$$

where

$$R(t) = r_p/\sin^2\frac{1}{2}\psi(t), \tag{A16}$$

and $\psi(t)$ is the true anomaly obeying the Kepler equation

$$\sqrt{\frac{Gm_{\rm bh}}{2r_p^3}}t = -\cot\frac{1}{2}\psi\left(1 + \frac{1}{3}\cot^2\frac{1}{2}\psi\right). \tag{A17}$$

With this, and using equation (A9), the integrals in equation (A14) can be evaluated to obtain the nonvanishing generalized forces

$$\begin{bmatrix} F_1(t) \\ F_2(t) \\ F_5(t) \end{bmatrix} = -3G\frac{m_{\rm bh}}{16r_p^3}\sqrt{\frac{3}{5\pi}}M_*R_*^2\sin^6\frac{1}{2}\psi\begin{bmatrix} \cos 2\psi \\ \sin 2\psi \\ -1/\sqrt{3} \end{bmatrix}. \tag{A18}$$

Finally, we write down the Euler-Lagrange equations of motion $[(d/dt)\partial L/\partial\dot{a}_k - \partial L/\partial a_k = Q_k]$ for modal amplitudes. After introducing the characteristic time $t_f = (2r_p^3/Gm_{\rm bh})^{1/2}$ and the dimensionless time $\tau = t/t_f$, they can be cast into the dimensionless form

$$\frac{d^2a_i}{d\tau^2} + (\omega_q t_f)^2 a_i = f_i(\tau), \tag{A19}$$

where the dimensionless forces $f_i(\tau)$ are functions of $\psi(\tau)$ only:

$$\begin{pmatrix} f_1 \\ f_2 \\ f_5 \end{pmatrix} = -\frac{1}{4}\sqrt{\frac{3\pi}{5}}\sin^6\frac{1}{2}\psi\begin{pmatrix} \cos 2\psi \\ \sin 2\psi \\ -1/\sqrt{3} \end{pmatrix}. \tag{A20}$$

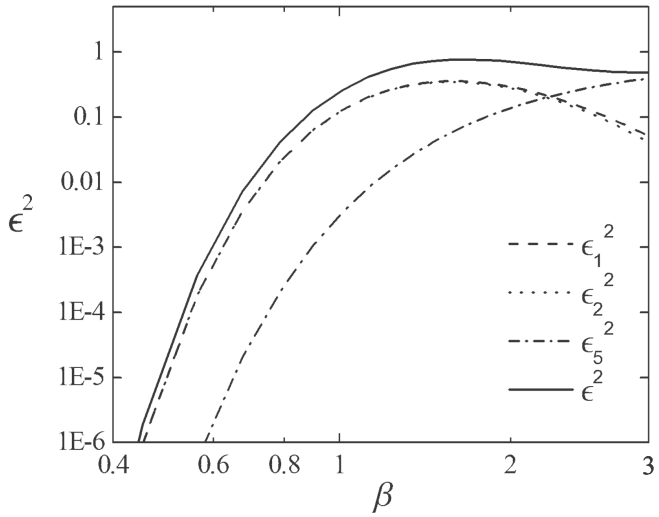

FIG. 7.—Effective eccentricity ε^2 as a function of the Roche penetration parameter. The lower three curves represent contributions from the three excited modes (1, 2, 5).

Thus, the only trace of parameters of the tidally interacting system is left in the factor $\omega_q t_f$, which is 2π times the ratio of the characteristic flyby time around the black hole and the period of quadrupole modes. It is useful to note that, using equations (1) and (A13), this product can be written as

$$\omega_q t_f = 8\sqrt{2/5}\left(r_p/r_{\rm R}\right)^{3/2} = 8\sqrt{2/5}(1/\beta)^{3/2}, \tag{A21}$$

i.e., it is inversely proportional to the power of the Roche radius penetration depth. In the case of a distant flyby $\omega_q t_f \gg 1$, so it follows from equation (A19) that $a_i = f_i(\omega_q t_f)^{-2} \propto m_{\rm bh}/\rho_* r_p^3$, which is the familiar result often used with Earth tides. Note, however, that for deep penetrations of the Roche radius $\omega_q t_f \leq 1$, and thus the (dimensionless) generalized forces $f_i(t)$ become large at frequencies that are resonant with ω_q.

We calculate the total work done by tidal forces on the system of normal modes during the whole flyby process by noting that it can formally be expressed as the change of the Hamiltonian $H(t) = T + U$ during the process (neglecting damping of normal modes). Initially, the quadrupole system starts in the undisrupted state with $H(t \to -\infty) = 0$, and it ends in a state of excited quadrupole modes[7] with $W_{\rm tide} = H(t \to \infty)$ (i.e., for $t \gg t_f$):

$$W_{\rm tide} = \frac{3}{4\pi} M_* R_*^2 \sum_{i=1}^{5} \lim_{t\to\infty} \left(\dot{a}_i^2 + \omega_q^2 a_i^2\right) = \sum_{i=1}^{5} \int_{-\infty}^{\infty} F_i(t)\dot{a}_i\, dt. \tag{A22}$$

Solving equation (A19) with the retarded Green's function, this can be written in the form

$$W_{\rm tide} = \frac{3}{4} G \frac{m_{\rm bh} M_* R_*^2}{r_p^3} \sum_{i=1}^{5} \left|\hat{\boldsymbol{f}}_i(\omega_q t_f)\right|^2, \tag{A23}$$

where

$$\hat{\boldsymbol{f}}_i(\Omega) = \frac{1}{\sqrt{2\pi}} \int_{-\infty}^{\infty} f(\tau) e^{i\Omega\tau}\, d\tau. \tag{A24}$$

We note that $W_{\rm tide}$ can be written in the form $G m_{\rm bh}\tilde{q}/r_p^3$, where $\tilde{q} = M_* R_*^2 \varepsilon^2$ and according to equation (A23),

$$\varepsilon^2 = \frac{3}{4} \sum_{i=1}^{5} \left|\hat{\boldsymbol{f}}_i(\omega_q t_f)\right|^2 \tag{A25}$$

can be thought of as an effective eccentricity of the star at the periastron. Figure 7 shows that ε can reach values of the order of 1 if a flyby is comparable to the dynamic timescale of the star. Note however that for deep Roche-radius penetrations our first-order perturbation model no longer applies; closer analysis shows that the model is applicable for $\omega_q t_f > 1$, i.e., for $\beta \lesssim 3$ (eq. [A21]).[8]

[7] This is assuming that the tidal kick did not break up the star by imparting to the surface layers a velocity that is higher than the escape velocity.

[8] We note that for $1 \lesssim \beta \lesssim 3$ the tidal energy is proportional to β^2, since $\varepsilon^2 \propto 1/\beta$. This is in agreement with the result of Lacy et al. (1982) and Carter & Luminet (1983).

Now we are in the position to estimate the high value of the right side of equation (A7) for this simple parabolic infall of an incompressible star. The left side starts at zero, when the star is still far from the black hole. As time goes on, the internal kinetic and potential energy change with the energy of the tidal modes, so the left side is greatest when all the tidal energy is in the kinetic energy of the wave. Thus, the maximum value, which is also the maximum value of the right side, equals $W_{\rm tide}$.

Even if the above analysis is valid, strictly speaking, for an incompressible star and in the approximation of independent (small amplitude) tidal modes, it does suggest the qualitative conclusion that the tidal interaction depends crucially on the ratio period of the fundamental mode versus typical flyby time ($\omega_q t_f$) and does become resonant if the flyby time is less than the period of the fundamental mode. The energy deposited into the star by the tidal interaction can be of the order of $G(m_{\rm bh}M_*R_*^2/r_p^3) = M_*c^2 r_g R_*^2/r_p^3$, which may surpass the absolute value of the internal gravitational energy of the star by many orders of magnitude if r_p, R_*, and r_g happen to be of the same order.

REFERENCES

Ayal, S., Livio, M., & Piran, T. 2000, ApJ, 545, 772
Baganoff, F. K., et al. 2001, Nature, 413, 45
Bowers, R. L., & Deeming, T. 1984, Astrophysics I: Stars (Boston: Jones and Bartlett)
Brajnik, M. 1999, BS thesis, Univ. Ljubljana
Čadež, A., Brajnik, M., Gomboc, A., Calvani, M., & Fanton, C. 2003, A&A, 403, 29
Čadež, A., & Gomboc, A. 1996, A&AS, 119, 293
Carroll, B. W., & Ostlie, D. A. 1996, An Introduction to Modern Astrophysics (Reading: Addison-Wesley)
Carter, B., & Luminet, J. P. 1982, Nature, 296, 211
———. 1983, A&A, 121, 97
———. 1985, MNRAS, 212, 23
Diener, P., Frolov, V. P., Khokhlov, A. M., Novikov, I. D., & Pethick, C. J. 1997, ApJ, 479, 164
Fulbright, M. S., Benz, W., & Davies, M. B. 1995, ApJ, 440, 254
Gezari, S., Halpern, J. P., Komossa, S., Grupe, D., & Leighly, K. M. 2003, ApJ, 592, 42
Goldstein, H. 1981, Classical Mechanics (Reading: Addison-Wesley)
Gomboc, A. 2001, Ph.D. thesis, Univ. Ljubljana
Gomboc, A., Fanton, C., Carlotto, L., & Čadež, A. 1999, in Recent Developments in Theoretical and Experimental General Relativity, Gravitation, and Relativistic Field Theories, ed. T. Piran & R. Ruffini (Singapore: World Scientific), 759
Grupe, D., Thomas, H.-C., & Leighly, K. M. 1999, A&A, 350, L31
Gurzadyan, V. G., & Ozernoy, L. M. 1981, A&A, 95, 39
Ivanov, P. B., Chernyakova, M. A., & Novikov, I. D. 2003, MNRAS, 338, 147
Ivanov, P. B., & Novikov, I. D. 2001, ApJ, 549, 467
Khokhlov, A., Novikov, I. D., & Pethick, C. J. 1993a, ApJ, 418, 163
———. 1993b, ApJ, 418, 181
Kochanek, C. S. 1994, ApJ, 422, 508
Komossa, S., & Bade, N. 1999, A&A, 343, 775
Lacy, J. H., Townes, C. H., & Hollenbach, D. J. 1982, ApJ, 262, 120
Laguna, P., Miller, W. A., Zurek, W. H., & Davies, M. B. 1993, ApJ, 410, L83
Loeb, A., & Ulmer, A. 1997, ApJ, 489, 573
Luminet, J. P., & Marck, J. A. 1985, MNRAS, 212, 57
Magorrian, J., & Tremaine, S. 1999, MNRAS, 309, 447
Marck, J. A., Lioure, A., & Bonazzola, S. 1996, A&A, 306, 666
Rees, M. J. 1988, Nature, 333, 523
———. 1990, Science, 247, 817
Renzini, A., Greggio, L., di Serego-Alighieri, S., Cappellari, M., Burstein, D., & Bertola, F. 1995, Nature, 378, 39
Schödel, R., et al. 2002, Nature, 419, 694
Swihart, T. L. 1971, Basic Physics of Stellar Atmospheres (Tucson: Pachart)
Syer, D., & Ulmer, A. 1999, MNRAS, 306, 35